JCI The Journal of Clinical Investigation

Ciliogenesis is regulated by a huntingtin-HAP1-PCM1 pathway and is altered in Huntington disease

Guy Keryer, … , Ioannis Dragatsis, Frédéric Saudou

J Clin Invest. 2011;121(11):4372-4382. https://doi.org/10.1172/JCI57552.

Research Article

Huntington disease (HD) is a devastating autosomal-dominant neurodegenerative disorder. It is caused by expansion of a CAG repeat in the first exon of the huntingtin (*HTT*) gene that encodes a mutant HTT protein with a polyglutamine (polyQ) expansion at the amino terminus. Here, we demonstrate that WT HTT regulates ciliogenesis by interacting through huntingtin-associated protein 1 (HAP1) with pericentriolar material 1 protein (PCM1). Loss of Htt in mouse cells impaired the retrograde trafficking of PCM1 and thereby reduced primary cilia formation. In mice, deletion of Htt in ependymal cells led to PCM1 mislocalization, alteration of the cilia layer, and hydrocephalus. Pathogenic polyQ expansion led to centrosomal accumulation of PCM1 and abnormally long primary cilia in mouse striatal cells. PCM1 accumulation in ependymal cells was associated with longer cilia and disorganized cilia layers in a mouse model of HD and in HD patients. Longer cilia resulted in alteration of the cerebrospinal fluid flow. Thus, our data indicate that WT HTT is essential for protein trafficking to the centrosome and normal ciliogenesis. In HD, hypermorphic ciliogenesis may affect signaling and neuroblast migration so as to dysregulate brain homeostasis and exacerbate disease progression.

 Related Commentary, page 4237

Ciliogenesis is regulated by a huntingtin-HAP1-PCM1 pathway and is altered in Huntington disease

Guy Keryer,[1,2,3] Jose R. Pineda,[1,2,3] Géraldine Liot,[1,2,3] Jinho Kim,[4] Paula Dietrich,[5] Caroline Benstaali,[1,2,3] Karen Smith,[4] Fabrice P. Cordelières,[1,6] Nathalie Spassky,[7] Robert J. Ferrante,[4] Ioannis Dragatsis,[5] and Frédéric Saudou[1,2,3]

[1]Institut Curie, [2]CNRS UMR3306, and [3]INSERM U1005, Orsay, France. [4]Department of Neurological Surgery, Neurology and Neurobiology, University of Pittsburgh, Pittsburgh, Pennsylvania, USA. [5]Department of Physiology, The University of Tennessee, Health Science Center, Memphis, Tennessee, USA. [6]IBISA Cell and Tissue Imaging Facility, Orsay, France. [7]Institut de Biologie de l'Ecole Normale Supérieure (IBENS), INSERM U1024, CNRS UMR8197, Paris, France.

Huntington disease (HD) is a devastating autosomal-dominant neurodegenerative disorder. It is caused by expansion of a CAG repeat in the first exon of the huntingtin (*HTT*) gene that encodes a mutant HTT protein with a polyglutamine (polyQ) expansion at the amino terminus. Here, we demonstrate that WT HTT regulates ciliogenesis by interacting through huntingtin-associated protein 1 (HAP1) with pericentriolar material 1 protein (PCM1). Loss of Htt in mouse cells impaired the retrograde trafficking of PCM1 and thereby reduced primary cilia formation. In mice, deletion of Htt in ependymal cells led to PCM1 mislocalization, alteration of the cilia layer, and hydrocephalus. Pathogenic polyQ expansion led to centrosomal accumulation of PCM1 and abnormally long primary cilia in mouse striatal cells. PCM1 accumulation in ependymal cells was associated with longer cilia and disorganized cilia layers in a mouse model of HD and in HD patients. Longer cilia resulted in alteration of the cerebrospinal fluid flow. Thus, our data indicate that WT HTT is essential for protein trafficking to the centrosome and normal ciliogenesis. In HD, hypermorphic ciliogenesis may affect signaling and neuroblast migration so as to dysregulate brain homeostasis and exacerbate disease progression.

Introduction

Huntington disease (HD) is an autosomal-dominant neurodegenerative disorder caused by the pathogenic expansion of the polyglutamine (polyQ) N-terminal stretch in the huntingtin protein (HTT; encoded by *HTT*). HD is characterized by the dysfunction and death of neurons in the brain, leading to devastating cognitive, psychiatric, and motor symptoms in patients. Studies in multiple cell and animal model systems support the notion that polyQ expansion in mutant Htt leads to the gain of new toxic functions and loss of the neuroprotective functions of the WT Htt (1).

Although some of its functions are linked to transcriptional activities in health and disease, Htt is primarily a cytoplasmic protein that associates with microtubules (MTs) and vesicles. Htt regulates intracellular trafficking of various organelles, including vesicles, by interacting with the dynein/dynactin pathway (2–4). Htt facilitates MT-dependent transport by interacting directly with dynein (2) and indirectly via huntingtin-associated protein 1 (HAP1), which binds to the dynactin p150^{Glued} subunit (3, 5–7). In pathological situations, the Htt-HAP1-dynactin complex is altered, resulting in a reduction of vesicular transport in neurons (3). These findings show that Htt integrates vesicular transport by regulating the activity of specific protein complexes containing the dynein/dynactin and kinesin 1 complexes and adaptor proteins such as HAP1.

With 2 patterns of axonemal MTs (9 + 0 in primary cilia and 9 + 2 in motile cilia), cilia are involved in sensory role, motility, and flow generation. Within the last 5 years, the importance of this organelle was highlighted by linking mutations within proteins of the cilia and ciliary basal bodies to a class of complex syndromes now termed ciliopathies (reviewed in 8). Whereas primary cilium originates from the mother centriole of the centrosome, which becomes the basal body, motile cilia of multiciliated or ependymal cells rely on the massive de novo formation of basal bodies from fibrous aggregates termed deuterosomes. Although they have different functions, primary and motile cilia share common properties. Cilia biogenesis depends on the trafficking of protein complexes to the pericentriolar material (PCM), a nonmembranous protein lattice that surrounds the centrioles and serves as a structural matrix to nucleate and anchor MTs. Pericentriolar material 1 protein (PCM1) is the major component of the centriolar satellites that shuttle between the cytoplasm and the PCM along MT in a dynein-dependent manner (9).

Proper trafficking and localization of PCM proteins such as PCM1 regulates ciliogenesis. Depleting PCM1 reduces ciliogenesis, and knockdown or mutation of BBS4 leads to PCM1 mislocalization and reduced ciliation both in vitro and in vivo (10–12). Mutation of CEP290, which underlies Joubert syndrome and results in a ciliopathy, depletes PCM1 from the centrosome and reduces ciliogenesis (10). These studies highlight the role of PCM1 trafficking for proper cilia biogenesis. Interestingly, PCM1 has been reported to interact with HAP1 (5), suggestive of a possible link between Htt and PCM1.

In the brain ventricles, motile cilia play a crucial role in circulating cerebrospinal fluid (CSF) inside the brain cavities. CSF is produced largely by the choroid plexus (CP) and circulates from the lateral to the third and fourth ventricles and then into the spinal and subarachnoid spaces (13). CSF contains ions, nutrients, neuroendocrine factors, and neurotransmitters, and a key func-

Authorship note: Guy Keryer and Jose R. Pineda contributed equally to this work.
Conflict of interest: The authors have declared that no conflict of interest exists.
Citation for this article: *J Clin Invest.* 2011;121(11):4372–4382. doi:10.1172/JCI57552.

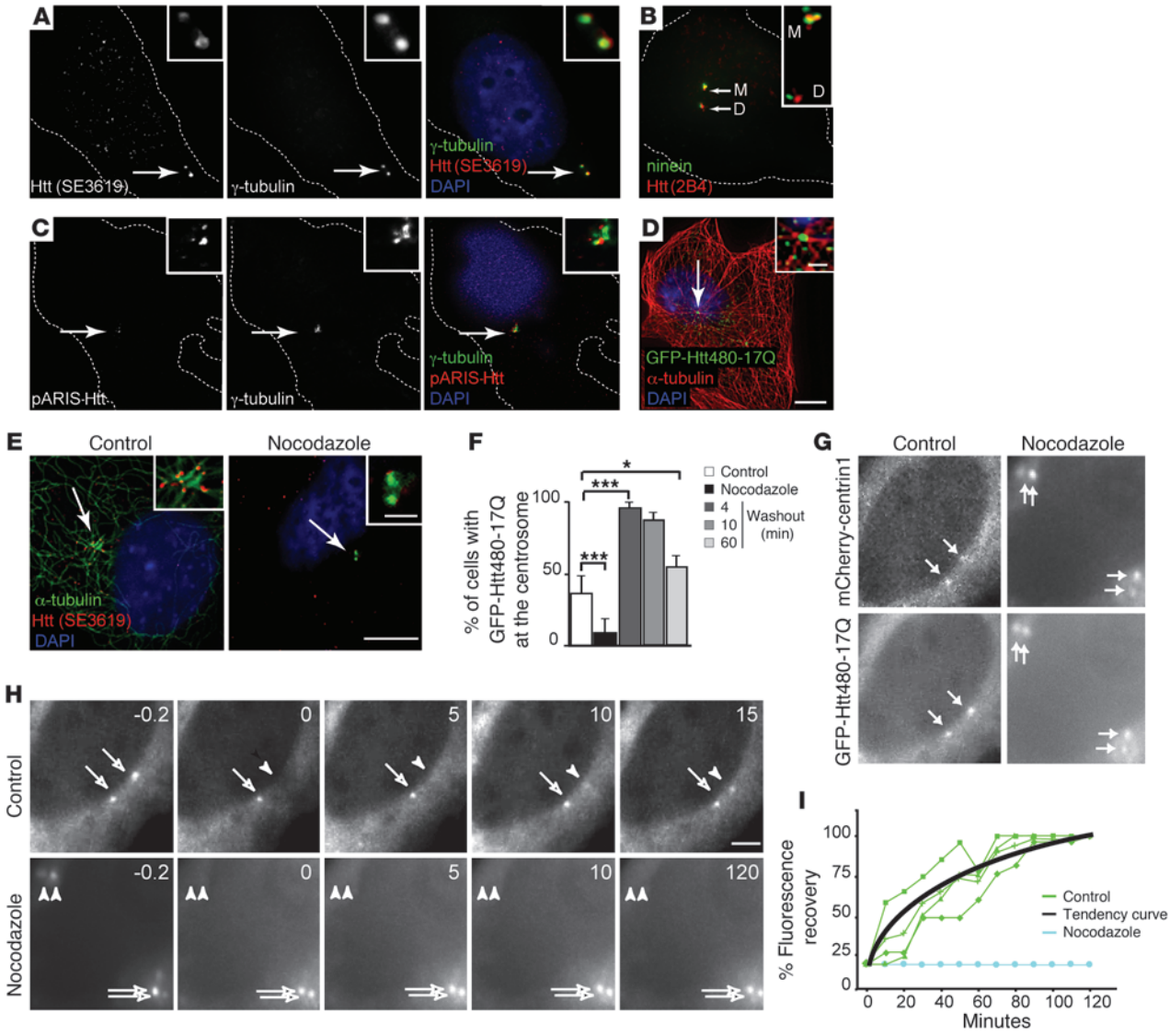

Figure 1

Htt associates with centrosome in a MT-dependent manner in mouse ST*Hdh*$^{+/+}$ cells. (**A**) Immunostaining with anti-Htt (SE3619) and anti–γ-tubulin and (**B**) anti-ninein and anti-Htt (2B4) Abs. (**C**) Anti–γ-tubulin immunostaining of cells expressing pARIS-mCherry-Htt. (**D**) Anti–α-tubulin immunostaining of cells expressing GFP-Htt480-17Q. (**E**) Immunostaining of cells in control condition or after MT depolymerization (nocodazole) with anti-Htt (SE3619) and anti–α-tubulin Abs. (**A**–**E**) Cells were counterstained with DAPI. (**F**) Quantification of GFP-Htt480-17Q at centrosome in control or nocodazole conditions and after different washout times. $n = 3$; 750 cells per condition. *$P < 0.05$; ***$P < 0.001$. (**G**) Representative cells expressing mCherry-centrin1 and GFP-Htt480-17Q. The nocodazole-treated cell was in G2 phase (duplicated centrosomes). (**H**) Representative FRAP experiment of GFP-Htt480-17Q transfected cells in control or nocodazole conditions. (**I**) FRAP graph. Tendency curve was calculated for 4 bleached centrioles in control condition. Arrows in **A**, **C**–**E**, **G**, and **H** denote the centrosome. Scale bars: 5 μm; 1 μm (insets).

tion of its flow is the clearance of brain catabolites. The total CSF volume is about 160 ml in humans, and this is replaced about 4 times per day, illustrating the important role of CSF circulation in brain homeostasis. However, in the aging CNS and in Alzheimer disease, CSF flow and turnover are reduced, resulting in a reduced clearance of potentially toxic catabolites (13). Altered CSF production from the CP (14) or defects in ependymal flow as a result of dysmotile cilia (15) result in aqueduct stenosis and hydrocephalus. In mice, specific deletion of Htt in the Wnt-1 lineage results in congenital hydrocephalus, which suggests that Htt could play a role in the regulation of CSF homeostasis (16).

We demonstrate here that Htt localizes at the centrosome through an MT-dependent transport and forms a complex with PCM1 and HAP1 proteins. Depletion of Htt or HAP1 led to dispersion of PCM1 from centrosomes and reduced ciliogenesis in cells. Ablation of Htt in the Wnt-1 lineage reduced ciliogenesis in vivo and led to hydrocephalus in mice. In contrast, pathological polyQ expansion concentrated PCM1 at the centrosome, resulting in increased ciliogenesis. Finally, abnormal ciliation of the ependymal layer in the wall of the lateral ventricles in HD knockin mice and in HD patients was associated with asynchronous beating of the cilia and abnormal CSF flow in HD mice.

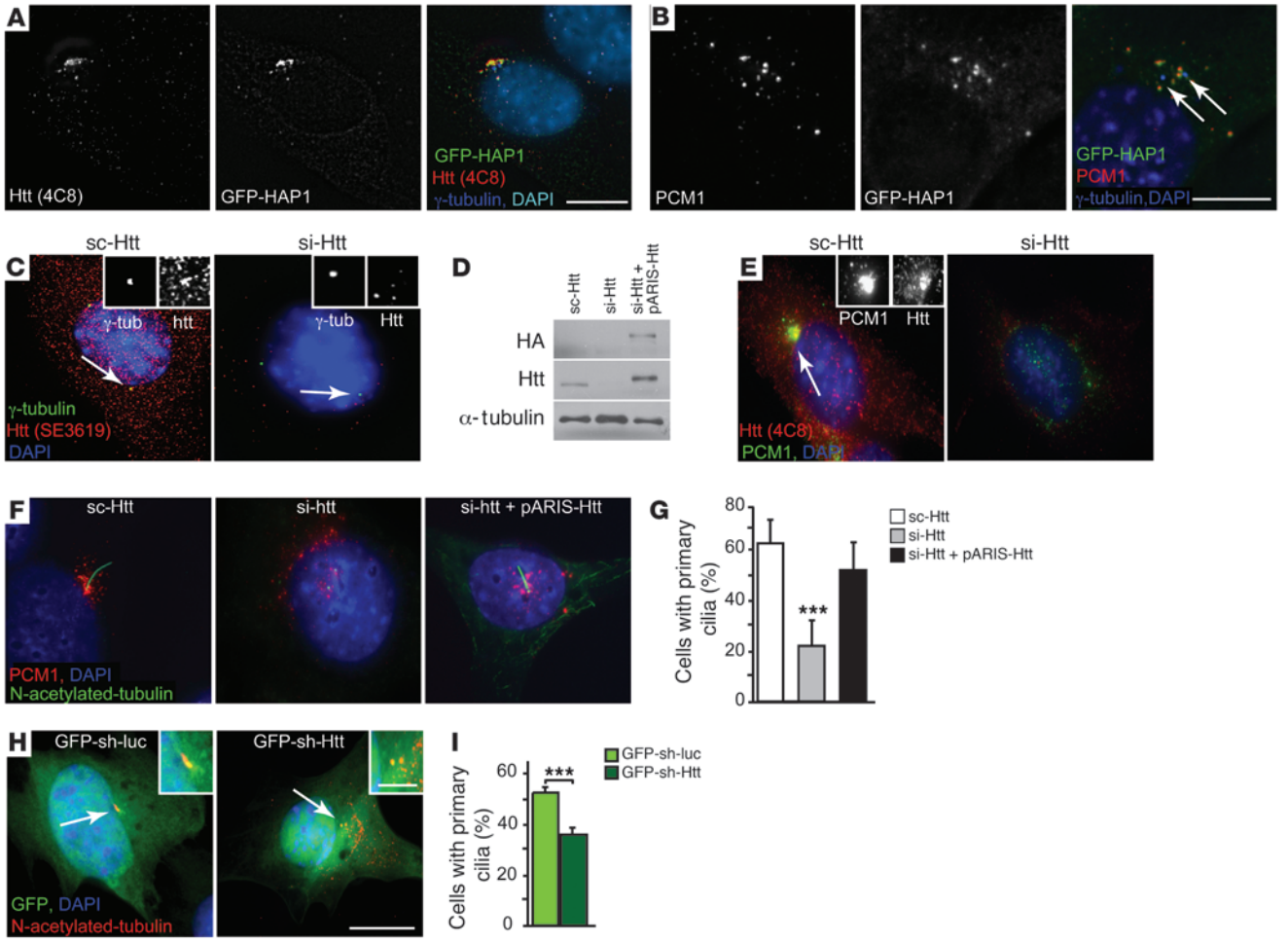

Figure 2

Htt depletion mislocalizes PCM1 and impairs primary cilia formation in striatal cells. (**A** and **B**) Immunostaining of GFP-HAP1–transfected cells (**A**) for Htt (4C8) and γ-tubulin and (**B**) for PCM1. Arrows denote γ-tubulin staining. (**C**) Immunostaining of cells treated with scrambled RNA (sc-Htt) or siRNA targeting Htt (si-Htt) for Htt (SE3619) and γ-tubulin. (**D**) Immunoblotting of lysates from sc-Htt cells, si-Htt cells, and si-Htt cells expressing pARIS-Htt. (**E**) Immunostaining of sc-Htt or si-Htt cells with anti-Htt (4C8) and PCM1 Abs. (**F**) Immunostaining of cells transfected with sc-Htt, si-Htt, and si-Htt with pARIS-Htt for PCM1 and N-acetylated tubulin. (**G**) Quantification of primary cilia in cells as in **F**. $n = 4$; at least 1,227 cells per condition. ***$P < 0.0001$. (**H**) Immunostaining of cells transfected with GFP-sh-luciferase (GFP-sh-luc) and GFP-sh-Htt for N-acetylated tubulin. (**I**) Quantification of primary cilia in cells as in **H**. $n = 2$, at least 430 cells per condition. ***$P = 0.001$. (**A**–**H**) Cells were counterstained with DAPI. Scale bars: 5 μm; 1 μm (insets).

Results

Htt localizes at centrosomes. We analyzed the localization of Htt in mouse neuronal cells immortalized from striatal neurons (referred to herein as ST*Hdh*$^{+/+}$ cells) (17). To selectively label the fraction of Htt associated with the cytoskeleton, we first permeabilized cells before fixation, as most of Htt is found in the cytosolic fraction (3, 4). We found Htt to be enriched at the centrosome, as shown by colocalization with γ-tubulin (Figure 1A). Similar localization was observed using another Htt Ab raised against a different epitope of Htt (Figure 1B and ref. 18). We also found Htt to be enriched at the centrosome in human retinal pigment epithelial cells (hTERT-RPE1) and in CHO and HEK 293 cells (Supplemental Figure 1, A–D; supplemental material available online with this article; doi:10.1172/JCI57552DS1). We further analyzed Htt localization using a synthetic full-length Htt fused to mCherry protein (pARIS-Htt; Figure 1C and ref. 7) and an N-terminal 480–amino acid fragment of Htt with a normal polyQ stretch fused to GFP (GFP-Htt480-17Q; Figure 1D). In both cases, we observed exogenous Htt in the vicinity or at centrosomes. We next expressed constructs that do not contain the HAP1 protein-binding domain and found that these constructs did not localize at the centrosome (Supplemental Figure 1, E–G). We immunostained cells for Htt and ninein, a specific marker of the mother centrioles (19), and found that Htt associated with both mother and daughter centrioles in ST*Hdh*$^{+/+}$ (Figure 1B) and hTERT-RPE1 cells (Supplemental Figure 1D).

Htt centrosomal localization is MT dependent. Most of the centrosomes (50%–80%) in nontreated cells were immunopositive for Htt (Figure 1E). However, complete MT depolymerization, as shown by the loss of α-tubulin staining, led to the depletion of Htt at the centrosome. In addition, MT depolymerization of ST*Hdh*$^{+/+}$ cells expressing GFP-Htt480-17Q induced loss of Htt centrosomal localization (Figure 1F). We next induced MT repolymerization

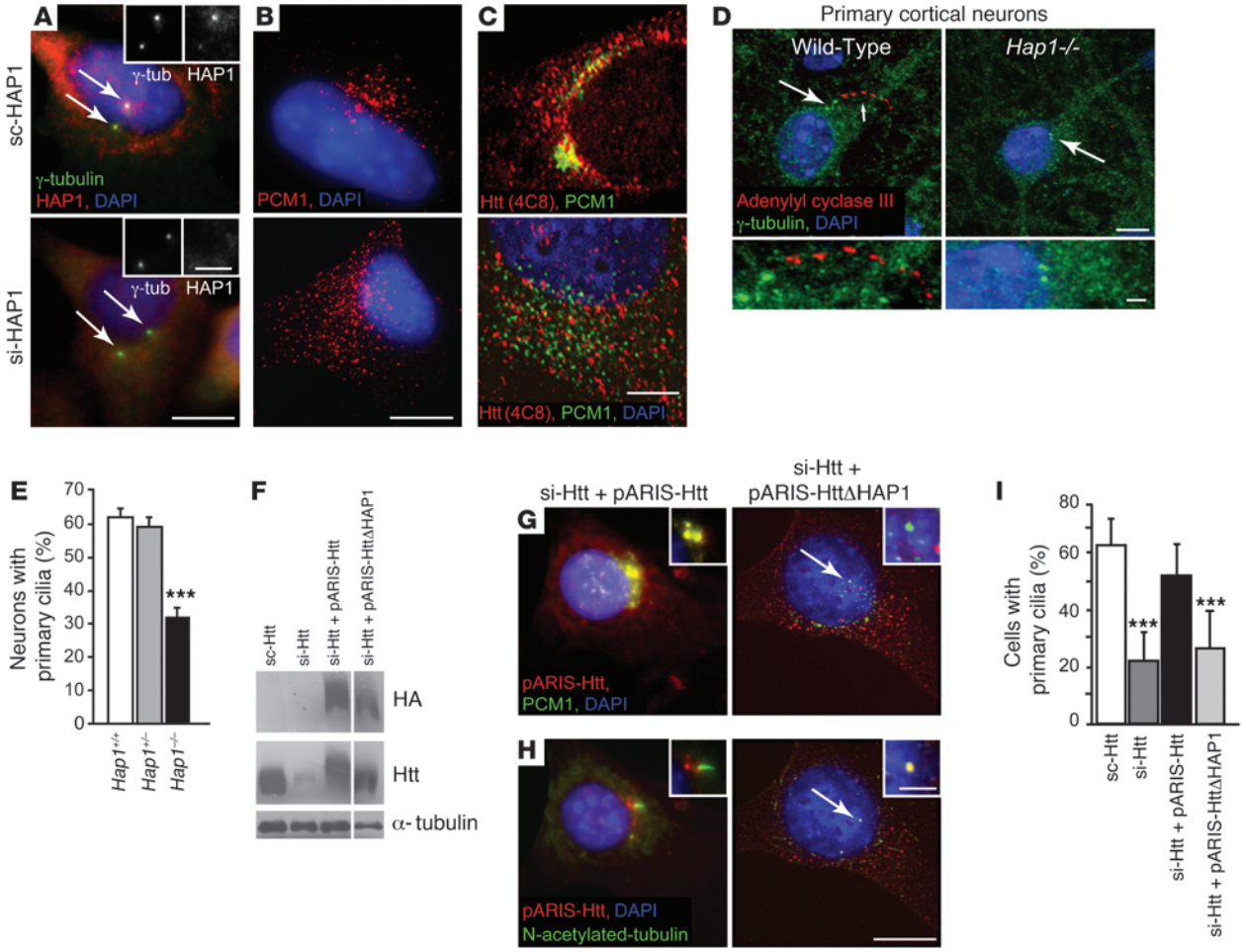

Figure 3

Htt regulates PCM1 distribution and ciliogenesis via HAP1. (**A**–**C**) ST*Hdh*$^{+/+}$ cells were electroporated with scrambled HAP1 (sc-HAP1) or siRNA targeting HAP1 (si-HAP1). Shown is immunostaining for HAP1 and (**A**) γ-tubulin, (**B**) PCM1, (**C**) and Htt (4C8) and PCM1. (**D**) Primary cortical neurons from WT or *Hap1*$^{-/-}$ mice were immunostained for adenylyl cyclase III and γ-tubulin. Large arrow indicates the position of centrosome (green dots); small arrow indicates adenylyl cyclase III–immunopositive cilium. (**E**) Quantification of primary cilia in neurons from WT (n = 1,062), *Hap*$^{+/-}$ (n = 1,065), and *Hap1*$^{-/-}$ (n = 1,312) mice as in **D** (n = 5 mice per genotype). ***P < 0.0001. (**F**) Immunoblotting of lysates from sc-Htt cells, si-Htt cells, or si-Htt cells expressing pARIS-Htt or pARIS-HttΔHAP1. Lanes were run on the same gel but were noncontiguous (white line). (**G**) PCM1 immunostaining of cells electroporated with si-Htt plus pARIS-Htt or si-Htt with the pARIS-HttΔHAP1 vector. (**H**) N-acetylated tubulin immunostaining of cells as in **G**. Arrows in **G** and **H** denote the position of centrioles. (**I**) Quantification of primary cilia (at least 610 cells per condition) as in **H**. ***P < 0.0001. (**A**–**C**, **D**, **G**, and **H**) Cells were counterstained with DAPI. Scale bars: 5 μm; 1 μm (inset).

and observed relocalization of GFP-Htt480-17Q after only 4 minutes of MT regrowth. The frequency of GFP-tagged Htt at the centrosome then decreased back to control values, which suggests a MT-dependent dynamic process.

We then performed fluorescence recovery after photobleaching (FRAP) experiments. ST*Hdh*$^{+/+}$ cells expressing mCherry-centrin1 as a marker of centrioles and GFP-Htt480-17Q showed a centrosomal localization of both constructs (Figure 1G). Next, we photobleached one centriole of the centrosome pair in the control situation and one pair of centrioles in the nocodazole-treated cell (5 μM, 1 hour; cell in G2 phase) and analyzed fluorescence recovery (Figure 1, H and I, and Supplemental Videos 1 and 2). Under control conditions, GFP FRAP was observed at the centrosome between 15 and 60 minutes ($t_{1/2}$, 30 minutes). However, with nocodazole treatment, no recovery was observed for up to 2 hours. Thus, Htt dynamically localized at the centrosome in a MT-dependent manner.

Htt associates with HAP1 and PCM1 at the centrosome. We observed that endogenous Htt localized with HAP1 at the centrosome and at pericentriolar satellites in cells expressing GFP-HAP1 (Figure 2A). This colocalization was in agreement with Htt and HAP1 localizations at the spindle poles during mitosis (18, 20). Endogenous PCM1 colocalized with GFP-HAP1 (Figure 2B) and with endogenous Htt (Figure 2E), and Htt localized with PCM1 satellites at the centrosome in cells expressing pARIS-Htt (Supplemental Figure 2A) or the GFP-Htt480-17Q construct (Supplemental Figure 2B). Analysis of PC12 cells that stably express GFP-HAP1 showed a significant codistribution of GFP-HAP1 with PCM1 (Supplemental Figure 2C). Immunoprecipitation of HAP1 using an anti-GFP Ab detected an interaction among HAP1, PCM1, and

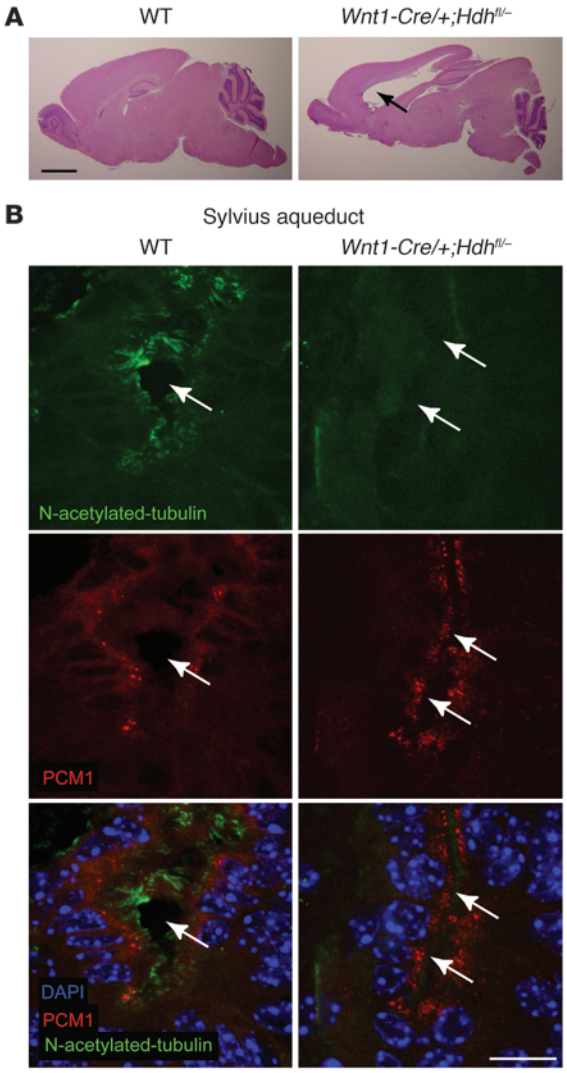

Figure 4
Mice lacking Htt in ependymal cells show altered PCM1 distribution, ciliary defects, and hydrocephalus. (**A**) Hematoxylin and eosin staining of sagittal sections of WT, *Wnt1-Cre/+;Hdh*$^{fl/-}$ mice revealed hydrocephalus phenotype in mice lacking Htt. Black arrows indicate hydrocephalus in mutant mice. (**B**) Immunofluorescence of brain coronal sections showing the Sylvius aqueduct from P15 WT and *Wnt1-Cre/+;Hdh*$^{fl/-}$ mice stained for N-acetylated tubulin and PCM1 and counterstained for DAPI. Single arrows indicate the aqueduct in WT mice; parallel arrows indicate aqueduct stenosis in mutant mice. Scale bars: 2 mm (**A**); 10 μm (**B**).

Htt (Supplemental Figure 2D). Together with previous studies (5, 21), our present findings indicate that Htt, HAP1, and PCM1 interact and localize at the centrosome.

Htt depletion leads to dispersion of PCM1 satellites and impairs primary cilia formation. We next tested whether dysregulating Htt could alter PCM1 dynamics and consequently ciliogenesis. Downregulation of Htt by RNAi was reduced drastically Htt in cells, as shown by immunoblotting experiments (Figure 2D), and more specifically at the centrosome, as shown by the loss of Htt and the persistence of γ-tubulin staining cells (Figure 2C). Strikingly, in the absence of Htt, we observed a marked dispersion of PCM1 from the perinuclear region (Figure 2, E and F). This effect was observed with the use of another RNAi and of shRNA targeting different Htt sequences (data not shown). We also observed similar PCM1 dispersion when expressing ectopically GFP-PCM1 in Htt-depleted cells (data not shown).

We next investigated the effect of downregulating Htt on cilia formation. Cells were electroporated with si-Htt or a shRNA targeting a different Htt sequence (Figure 2, F and H) and were serum starved for 48 hours to induce primary cilia formation. We quantified the presence of primary cilia after staining the cells with N-acetylated tubulin Ab (Figure 2, F–I). There was a significant decrease in the percentage of cells with primary cilia in Htt-depleted compared with control cells. Finally, reexpressing pARIS-Htt, which is insensitive to si-Htt, restored PCM1 distribution at the centrosome and cilia formation in Htt-depleted cells (Figure 2, F and G). Therefore, Htt is essential in vitro for cilia biogenesis by regulating PCM1 distribution at the centrosome.

The Htt-HAP1-PCM1 pathway regulates ciliogenesis. We further investigated whether Htt mediates its effect on ciliogenesis through HAP1 protein. Silencing HAP1 expression led to a decrease in HAP1 staining at the centrosome (Figure 3A) and to the dispersion of PCM1 centrosomal staining (Figures 3B). We also cultured primary neurons from newborn P1 WT and *Hap1*$^{-/-}$ mice. We used adenylyl cyclase III as a marker for cilia. Adenylyl cyclase III showed a typical punctate distribution, as it is a membrane-associated protein (Figure 3D and ref. 22). We found a significant reduction in the percentage of neurons that have cilia in primary cortical neurons from *Hap1*$^{-/-}$ mice compared with WT neurons (Figure 3, D and E).

We next found that depleting HAP1 in cells dissociated Htt from PCM1 (Figure 3C), further demonstrating that these proteins are in the same complex. To unequivocally demonstrate the importance of HAP1 in Htt-mediated effect on ciliogenesis, we expressed a version of full-length Htt in which the HAP1 binding domain is deleted. This construct, pARIS-HttΔHAP1, does not interact with HAP1 and is unable to mediate the trafficking of brain-derived neurotrophic factor (BDNF) or reform the Golgi apparatus after disruption of the MT network (7). We extended our gene replacement experiment in which Htt was silenced (Figure 2, F and G) but reexpressed pARIS-HttΔHAP1 (Figure 3F). Whereas pARIS-Htt colocalized with PCM1, pARIS-HttΔHAP1 did not (Figure 3G). Furthermore, in contrast with pARIS-Htt, pARIS-HttΔHAP1 was unable to rescue ciliation (Figure 3, H and I). These results demonstrated that the Htt-HAP1-PCM1 pathway is required for ciliogenesis.

Inactivation of the Htt gene in Wnt-1 cell lineage alters PCM1 distribution in ependymal cells, reduces ciliogenesis, and leads to hydrocephalus in mice. Tissue-specific ablation of Htt in the Wnt-1 cell lineage, which also contributes to dorsal midline-derived ependymal secretory structures, led to hydrocephalus in mice (ref. 16 and Figure 4A). The phenotype was linked to abnormalities of the CP and of the subcommissural organ (SCO), with stenosis of the Sylvius aqueduct that links the third and the fourth ventricles. We analyzed PCM1 distribution and formation of cilia in such mice. Whereas motile cilia that were immunopositive for N-acetylated tubulin were observed at the entrance of the aqueduct of Sylvius in P15 WT mice, we found deacetylated and shorter cilia associated with marked stenosis of the duct in *Wnt1-Cre/+;Hdh*$^{fl/-}$ mice (Figure 4B). Analysis of PCM1 distribution revealed a significant dispersion of PCM1 when Htt was inactivated, with loss of cytoplasmic apical distribution of PCM1 granules in the duct ependymocytes

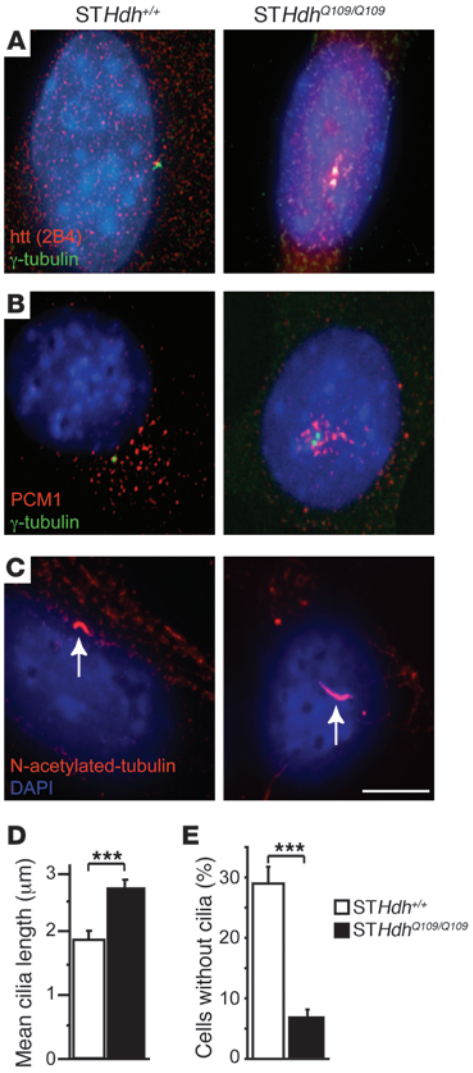

Figure 5
PolyQ-Htt aggregates PCM1 at centrosome and increases cilia length in striatal cells. (**A**–**C**) Immunostainings of mouse ST*Hdh*$^{+/+}$ and ST*Hdh*$^{Q109/Q109}$ cells for (**A**) Htt (2B4) and γ-tubulin, (**B**) PCM1 and γ-tubulin, and (**C**) N-acetylated tubulin showed abnormal accumulation of Htt (**A**), PCM1 (**B**), and increased length of cilia (**C**; arrows) in ST*Hdh*$^{Q109/Q109}$ cells. Cells were counterstained with DAPI. (**D**) Quantification of mean cilia length in ST*Hdh*$^{+/+}$ and ST*Hdh*$^{Q109/Q109}$ G0-arrested cells (70 cells per group). ***$P < 0.001$. (**E**) Quantification of ST*Hdh*$^{+/+}$ and ST*Hdh*$^{Q109/Q109}$ cells with no cilia. ***$P < 0.001$. Scale bar: 5 μm.

of *Wnt1-Cre/+;Hdh*$^{fl/-}$ compared with WT mice (Figure 4B). To ensure that cilia defects were not a consequence of longstanding hydrocephalus, we performed immunostaining on *Wnt1-Cre/+;Hdh*$^{fl/-}$ mice prior to the onset of overt hydrocephalus. In the dorsal population of ependymal cells at the level of the SCO, we observed a region that, in contrast to ventral cells, showed high Cre-mediated depletion of Htt (16), a specific loss of ciliated cells, whereas the ventral part had normal ciliated cells (Supplemental Figure 3, A and B). Thus, Htt depletion in vivo reduced cilia biogenesis. The hydrocephalus phenotype observed in these mice could therefore be caused by defects in CSF production from the CP and by defects in ciliation of ependymocytes within the duct leading to aqueduct stenosis.

Pathogenic polyQ-expanded Htt concentrates PCM1 at the centrosome and increases primary cilia length. We investigated the distribution of Htt and PCM1 in ST*Hdh*$^{+/+}$ cells and in their HD mutant counterparts (ST*Hdh*$^{Q109/Q109}$ cells; ref. 17). We observed an increased concentration of Htt at the centrosome and accumulation of PCM1-immunopositive centriolar satellites around the centrioles in ST*Hdh*$^{Q109/Q109}$ cells (Figure 5, A and B). Analysis of PCM1-GFP trafficking in living cells revealed that PCM1-GFP had a higher tendency to cluster at the centrosome in ST*Hdh*$^{Q109/Q109}$ versus ST*Hdh*$^{+/+}$ cells (Supplemental Video 3).

We next analyzed cilia length and found significantly longer cilia in ST*Hdh*$^{Q109/Q109}$ cells (Figure 5, C and D). In addition, the percentage of cells without cilia was lower in ST*Hdh*$^{Q109/Q109}$ cells (Figure 5E). We also investigated primary cilia formation in astrocytes from *Hdh*$^{Q111/Q111}$ mice and found a significant increase in the percentage of astrocytes with cilia compared with WT astrocytes (ref. 23 and Supplemental Figure 4). Together, these data showed that pathogenic polyQ expansion in Htt causes abnormal concentrations and decreased dynamics of PCM1 at the centrosome and increased ciliogenesis in neuronal cells and astrocytes.

HD knockin mice show PCM1 aggregation and increased ependymal cilia length. We next immunostained 12-month-old mouse brains for PCM1 and observed a striking accumulation of PCM1 in the CP of the third ventricle in *Hdh*$^{+/Q111}$ and *Hdh*$^{Q111/Q111}$ versus WT *Hdh*$^{+/+}$ mice (Figure 6, A–C, top). We then analyzed the ependymal layer of the lateral ventricles and observed accumulation of PCM1 in heterozygous and homozygous mutant mice (Figure 6, A–C, bottom). PCM1 was clustered in the apical part of the CP cells and of the ependymocytes in HD mice. We also observed a thickening of the cilia layer, as revealed by N-acetylated tubulin staining (Figure 6, A–C, bottom).

In the lateral ventricles, we found a progressive alteration in ciliogenesis, with marked aggregation of PCM1 detectable as early as 5 months and an altered cilia layer evident at 12 months (Supplemental Figure 5). We observed an earlier alteration in the CP with a significant increase in the N-acetylated tubulin–immunopositive layer as early as 1 month (Supplemental Figure 6). We therefore concluded that in HD mice, there is early alteration in PCM1 aggregation and in the size of the cilia layer in the CP and lateral ventricles, with some alterations detectable as early as 1 month in the CP.

We next performed scanning electron microscopy on mouse brains. There were no obvious differences in cilia number throughout the lateral wall between the different genotypes (data not shown). We measured the length and diameter of cilia under higher magnification (Figure 6D). Measurements were performed on various regions of the wall for each genotype to ensure that variation in length was not a result of cilia density (24). No significant differences were observed regarding the thickness of the cilia (WT, 0.213 ± 0.02 μm; mutant, 0.211 ± 0.01 μm; P = NS). However, we observed a statistically significant increase in cilia length in *Hdh*$^{+/Q111}$ and *Hdh*$^{Q111/Q111}$ mice compared with WT mice (Figure 6D). The cilia length in heterozygous and homozygous mice, although statistically different from each other, were close and markedly different from WT.

PCM1 and N-acetylated tubulin accumulate in HD patients. To examine the relevance of our findings to the pathogenesis of HD, we evaluated expression of PCM1 and N-acetylated tubulin in human HD

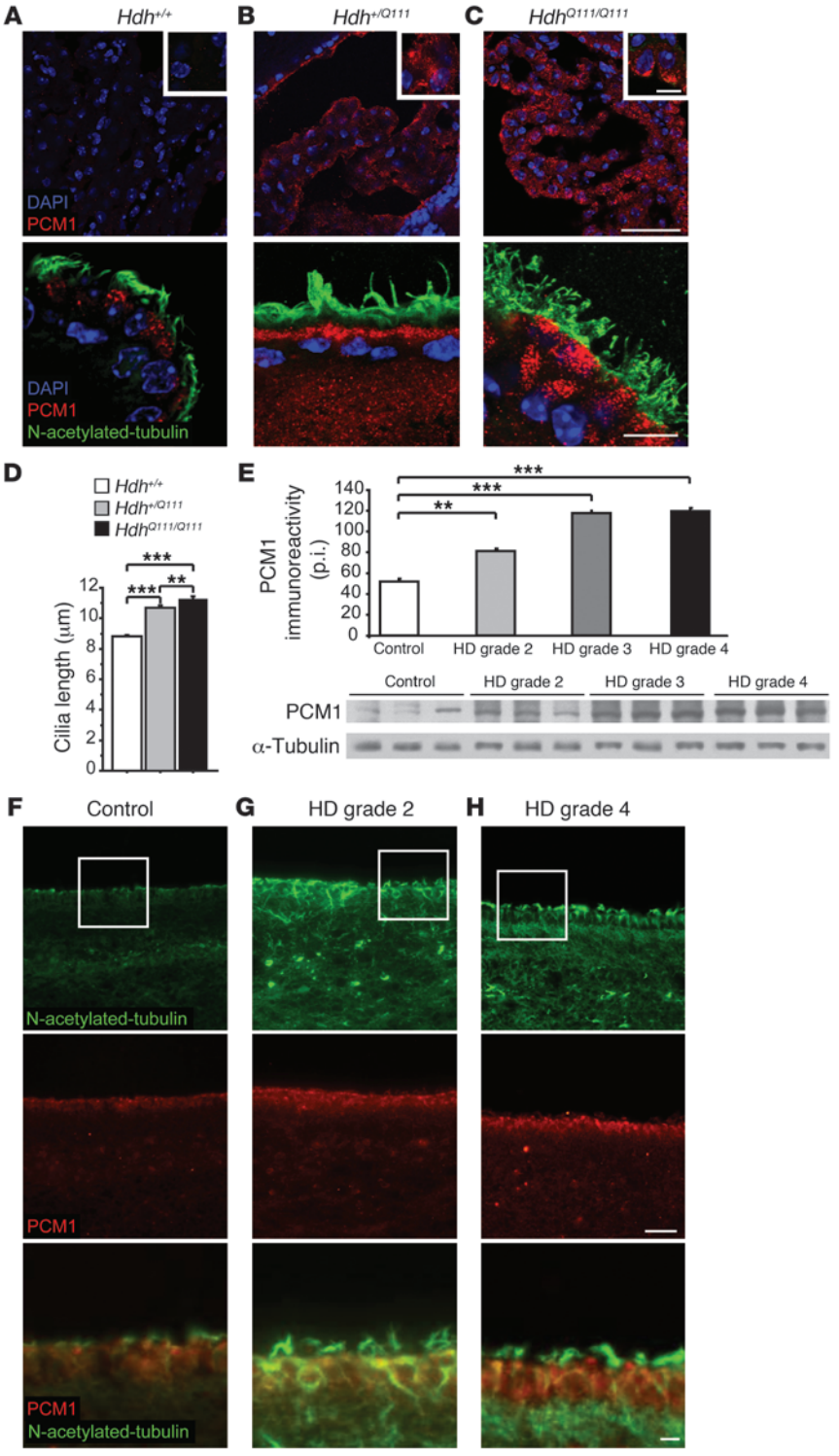

Figure 6

HD mice and patients show aggregation of PCM1 and increased ependymal cilia length. (**A**–**C**) Immunohistochemistry of mouse brain longitudinal sections from 1-year-old *Hdh*$^{+/Q111}$ (**B**) and *Hdh*$^{Q111/Q111}$ (**C**) mice showed accumulation of PCM1 in the CP (top) and of PCM1 and N-acetylated tubulin in the ependymal layer of the lateral ventricle (bottom) compared with WT mice (**A**). Scale bars: 50 μm (top); 10 μm (bottom); 4 μm (insets). (**D**) Increased cilia length in *Hdh*$^{+/Q111}$ (81 cilia) and *Hdh*$^{Q111/Q111}$ (180 cilia) compared with WT *Hdh*$^{+/+}$ (201 cilia) mice. $^{**}P = 0.001$; $^{***}P < 0.0001$. (**E**) Representative Western blot of human postmortem brain lysates from medial caudate nucleus at the ependymal border from HD grade 2, 3, and 4 subjects ($n = 8$ per group). Graph represents the quantification of PCM1 level in all 24 HD patients samples and 8 age-matched control subjects. p.i., pixel intensity. $^{**}P < 0.01$; $^{***}P < 0.0001$. (**F**–**H**) Representative striatal sections of HD grade 2 (**G**), HD grade 4 (**H**), and age-matched control (**F**) postmortem brain tissues, with the ependymal lateral ventricle zone showing increased immunoreactivity of N-acetylated tubulin (top) and of PCM1 (middle). Boxed regions are shown at higher magnification at bottom. Scale bars: 50 μm (top and middle); 10 μm (bottom).

neostriatal specimens. These specimens were from grade 2 and grade 4 HD cases, as defined by the Vonsattel criteria (25), and were paired with age-matched control specimens. Levels of immunostaining for both PCM1 and N-acetylated tubulin along the ependymal zone of the lateral ventricle in 10-μm-thick paraffin sections were higher than those in control specimens (Figure 6, F–H). Furthermore, Western blot analyses of frozen tissue samples from the ependymal zone of the lateral ventricle at the head of the caudate nucleus in grade 2, 3, and 4 HD cases showed a grade-dependent increase in PCM1 immunoreactivity (Figure 6E). These results indicate a marked alteration of the ependymal ciliated layer in HD patients.

Altered cilia orientation and impaired ependymal flow in HD mice. Although the absence of cilia leads to defects in CSF flow, the physiological consequences of abnormally long cilia is unknown.

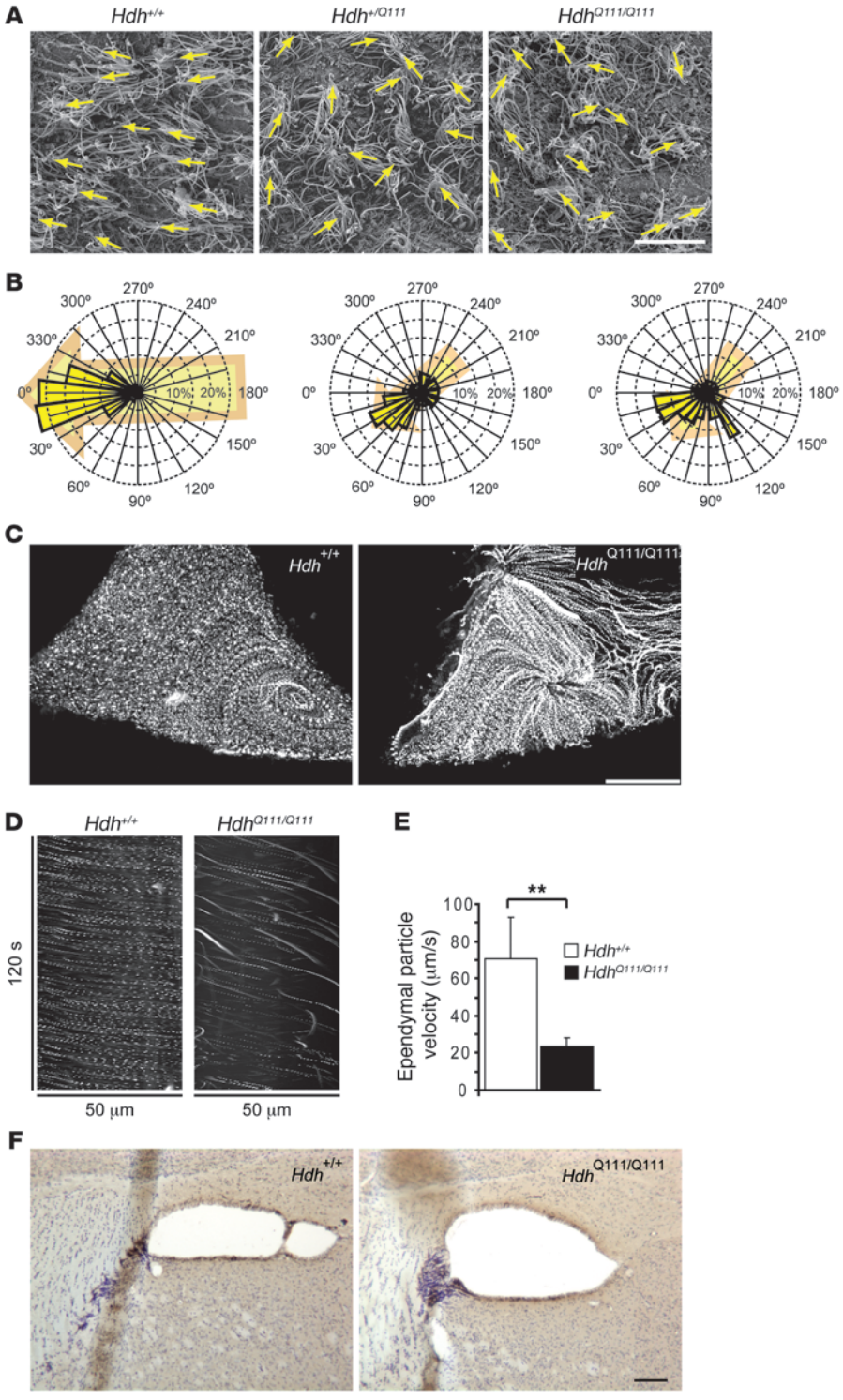

Figure 7

Ependymal cilia orientation and flow are altered in HD mice. (**A**) Scanning electron microscopy of lateral wall of the lateral ventricle from *Hdh*$^{+/+}$, *Hdh*$^{+/Q111}$, and *Hdh*$^{Q111/Q111}$ mice. Arrows indicate the orientation of the cilia tufts. Scale bar: 10 μm. (**B**) Distribution of cilia orientation around the mean (0°) in lateral ventricles from 3 each of *Hdh*$^{+/+}$ (380 tufts analyzed), *Hdh*$^{+/Q111}$ (465 tufts), and *Hdh*$^{Q111/Q111}$ (389 tufts) mice. (**C**) Ependymal trajectories of particles recorded in the lateral ventricle of 1-year-old *Hdh*$^{+/+}$ (1,532 particles) or *Hdh*$^{Q111/Q111}$ (1,055 particles) mice. Scale bar: 50 μm. (**D**) Representative kymographs. (**E**) Quantification of the velocity of particles generated by the ependymal flow. Velocity was calculated from 5 *Hdh*$^{+/+}$ mice and 9 *Hdh*$^{Q111/Q111}$ mice. $^{**}P < 0.01$. (**F**) DCX immunostaining along the RMS in coronal brain sections from *Hdh*$^{Q111/Q111}$ and *Hdh*$^{+/+}$ mouse brains. Scale bar: 100 μm.

We first analyzed the orientation of the cilia tufts on the lateral walls of the ventricles. In WT mice, most of the cilia were oriented toward the CSF flow (24, 26), whereas cilia in *Hdh*$^{+/Q111}$ and *Hdh*$^{Q111/Q111}$ mice were randomly oriented (Figure 7, A and B). As orientation of the cilia dictates flow directionality (26), we analyzed CSF flow by preparing organotypic coronal brain slices containing the lateral ventricle from 1-year-old mice. Sections were incubated with fluorescent microspheres and video recorded. Whereas flow was constant in the WT situation, with particles showing synchronous behavior, fluorescent particle flow was disorganized in *Hdh*$^{Q111/Q111}$ mice (Supplemental Videos 4 and 5). Stack projection of binarized microspheres revealed altered CSF flow in *Hdh*$^{Q111/Q111}$ mice (Figure 7C). Particles moved at the same speed in a synchronous fashion in WT mice, but were haphazard in *Hdh*$^{Q111/Q111}$ mice (Figure 7D). Furthermore, the average velocity of the particles was significantly reduced in the mutant mice (Figure 7E). These findings demonstrated a defect in cilia function and in CSF flow in HD.

Finally, to get insights into possible consequences of CSF fluid flow defects, we analyzed the rostral migratory stream (RMS) of new neurons in the brain, as neuroblasts were previously shown to follow the fluid flow in adult brain (26). To test this hypothesis, we performed DAB staining of doublecortin-immunopositive (DCX-immunopositive) neuroblasts in adult WT and *Hdh*$^{Q111/Q111}$ mice. The lateral ventricle, observed in coronal sections obtained from the anterior part of mouse brains, was more dilated in *Hdh*$^{Q111/Q111}$ than in WT mice. Moreover, DCX-immunopositive cells corresponding to migrating neuroblasts showed a marked alteration in their dorsal localization within the RMS (Figure 7F), with a marked concentration in the ventrolateral region of the lateral ventricle. These results suggest that CSF alteration in HD could potentially have dramatic consequences on brain homeostasis by altering the migration of new neurons.

Discussion

Htt and HAP1 regulate trafficking to the centrosome and cilium biogenesis. In the present study, we demonstrated that although Htt shuttles dynamically to the centrosome, it is not a bona fide centrosomal protein. Indeed, only a fraction of Htt localized at the centrosome (such as γ-tubulin or centrin; ref. 19). This amount was regulated, as shown by our FRAP experiments, and was dependent on an intact MT network. These observations — as well as the possibility that isolation procedures that use nocodazole are too stringent for Htt maintenance at centrosome (Figure 1F) — might also explain why Htt was not identified by mass spectrometry analyses in centrosomal preparations. Nevertheless, Htt may be essential in transporting protein complexes to the PCM and the base of the cilia. The role of Htt in trafficking of pericentriolar proteins may not be restricted to PCM1, as we consistently observed a dispersion of pericentrin and ninein in the absence of Htt and of HAP1. The BBS proteins also localize at the PCM, where they associate with PCM1 (11, 27). Whether the absence of Htt leads to defects in the localization of BBS proteins remains to be investigated. In contrast to BBS proteins, PCM1 did not traffic inside the cilium and remained in the PCM. This was similar to Htt, which was also not observed within the cilium.

Previous studies have reported that Htt controls trafficking of vesicles via a dynein/dynactin-dependent pathway (2–4). We propose here that Htt controls transport to the centrosome of proteins required for ciliogenesis. In the absence of Htt, dynein/dynactin-dependent transport would be altered, leading to a reduction of PCM proteins at the centrosome. In disease, the increased concentration of pericentriolar proteins is caused by the loss of the dynamics of pericentriolar satellites that remain closely localized to the centrosome (Supplemental Video 3). The altered dynamics of PCM1 are consistent with reduced trafficking of vesicles in HD (3).

Absence of Htt and HAP1 led to PCM1 dispersion and cilia defects. Whereas in vivo depletion of Htt led to absence of cilia and hydrocephalus, HAP1 knockout mice that survived to the feeding deficit phenotype do not exhibit this phenotype, as the SCO of *Hap1*$^{-/-}$ is normal with an intact aqueduct (28). These observations are also supported by studies indicating that cilia defects are not sufficient to cause hydrocephalus, but increase the risk of aqueduct closure (15).

An extending Htt-interacting network for ciliogenesis. The interacting network by which Htt regulates cilia dynamics and function could extend beyond HAP1 and PCM1 proteins. Cilia formation could also be affected by the interaction of Htt with the dynein/dynactin complex, which is involved in ciliogenesis (29). Indeed, Htt binds to dynein intermediate chain (2) and to p150^{Glued} via the HAP1 protein (3, 5, 6). Consistent with a functional interaction, we found a clustering of p150^{Glued} with PCM1 in ST*Hdh*$^{Q109/Q109}$ cells (data not shown).

In addition to PCM1, Htt-HAP1 could regulate other proteins involved in the control of ciliogenesis. HAP1 also interacts with the Ahi1 protein, and both colocalize in neurons with a perinuclear punctate structure (30). Ahi1 (also referred to as Jouberin) is found mutated in a significant percentage of individuals with Joubert syndrome, a disorder classified as a ciliopathy (29). Another pathway by which Htt could regulate ciliogenesis is the HIP1-Hippi pathway. Hippi is the human homolog of the intraflagellar protein IFT57 of *Chlamydomonas* and interacts with Htt-interacting protein 1 (HIP1) (29). Htt, HIP1, and Hippi have previously been identified in a proteome analysis of the mouse photoreceptor sensory cilium complex (31).

Mutant Htt and hypermorphic ciliogenesis phenotype. In the present study, we report defects in cilia length and organization in cellular and mouse models of HD and, more importantly, in HD patients. In HD mice, longer but misorientated cilia showed asynchronous beating, which led to abnormal CSF flow. Defects in fluid flow impair the migration of new neurons to the olfactory bulb (26). Interestingly, we observed a defect in the migration of neuroblasts along the RMS. This alteration could contribute to the olfactory abnormalities reported in HD patients and HD mice (32). The abnormal flow could also compromise the role of the CSF in clearing brain catabolites, raising the possibility of a defect in brain homeostasis in HD patients. In support of these observations, alterations in various factors and proteins have been detected in the CSF of HD patients (33). Such defects in brain clearance capacity could be deleterious and exacerbate the neuronal death observed in HD. Whether cilia alteration occurs in other tissues also remains to be investigated.

In addition to defects in motile cilia, we observed defects in primary cilia formation in neuronal cells and astrocytes. What are the consequences of such defects? Primary cilia are nonmotile but have a sensory role, regulating signaling pathways such as the hedgehog and PDGFα signaling pathways that are important to regulate organ development and homeostasis (8). Primary cilia could also be important for attenuating the Wnt signaling pathway through sequestration of β-catenin in the cilium together with Ahi1 (34). Interestingly, Htt interacts with β-catenin, and mutant Htt induces β-catenin accumulation in the cytoplasm (35). It will be of interest to investigate such pathways and determine to what extent cilia defect contributes to the large spectrum of symptoms in HD patients.

Our present findings revealed a role for Htt in regulating ciliogenesis. In disease, polyQ-Htt induces an effect opposite to that induced by loss of Htt function. Loss of the neuroprotective WT functions of Htt, as well as gain of new functions that are toxic to the cell, have been previously demonstrated to be involved in the etiology of the disease (1). For example, loss of Htt function in BDNF transcription and axonal transport contribute to disease by reducing trophic support to striatal neurons. In contrast, the presence of a short fragment of Htt that contains the polyQ expansion induces neurological phenotype in mice through the gain of new toxic mechanisms unrelated to Htt normal function. Indeed, only 2% of the Htt protein sequence with the expanded polyQ stretch is sufficient to induce neuronal degeneration, but such fragments are unable to stimulate transport in contrast to full-length constructs (3). Here we report a disease mechanism associated with a function of Htt that is hyperactivated in the disease situation and that corresponds to a hypermorphic ciliogenesis phenotype, a finding we believe to be novel. Whereas Htt deletion in vitro and in vivo resulted in loss of cilia, polyQ expansion in the context of the full-length Htt protein led to exacerbated function in cilia biogenesis. This mechanism involving exaggerated ciliogenesis further illustrates the complexity of the molecular mechanisms leading to this devastating disorder.

Methods

Cell lines, transfections, and treatments. 293T HEK (ATCC), CHO-K1 (ATCC), and infinity telomerase-immortalized human retinal pigment epithelial (h-TERT-RPE1; Clontech) cell lines were cultured as recommended by ATCC. The PC12 cell line stably expressing GFP-HAP1 was previously described (36). Mouse ST*Hdh*$^{+/+}$ and ST*Hdh*$^{Q109/Q109}$ cells were established from WT and *Hdh*$^{Q111/Q111}$ knockin mice and cultured as described previously (17). Cells were electroporated using cell line nucleofactor kit (Amaxa). ST*Hdh*$^{+/+}$ cells were treated with 4 μM nocodazole for 1 hour and then incubated for 30 minutes at 4°C to depolymerize MTs. For primary cilia induction,

ST*Hdh* cells were shifted from 10% to 0.2% serum 24 hours after siRNA treatment and fixed 48 hours later; primary astrocytes were shifted to DMEM without serum for 48 hours. The presence or absence of primary cilia was determined in a blinded manner with respect to cell genotype.

Constructs and siRNAs oligonucleotides. GFP-HttExon1, GFP-Htt480-17Q, and pARIS-mCherry-HttQ23 and pARIS-mCherry-HttQ23ΔHAP1 (referred to herein as pARIS-Htt and pARIS-HttΔHAP1, respectively) were previously described (4, 7). The GFP-Htt587-3144 construct was made by inserting a KpnI/SacII fragment of pcDNA-Htt586-3144 (gift from N. Déglon, CEA, Fontenay, France) into pEGFP-C1 vector (Clontech). pEGP-HAP1-A was a gift from X.J. Li (Emory University, Atlanta, Georgia, USA); PCM1-GFP was a gift from A. Merdes (CNRS, Toulouse, France); and mCherry-Centrin1 was a gift from A. Rousselet (Institut Curie, Paris, France). The RNA oligonucleotides for siRNA targeting mouse Htt or HAP1 have been previously used (3, 7). GFP-sh-Htt was from N. Déglon.

Mice. Generation and genotyping of *Wnt1-Cre/+;Hdh*$^{fl/-}$ mice (16), *Hap1*$^{-/-}$ mice (a gift from S.H. Li and X.J. Li, Emory University, Atlanta, Georgia, USA; ref. 36), and *Hdh*$^{Q111/Q111}$ mice (23) have been previously described. Animals were maintained with access to food and water ad libitum in a colony room kept at constant temperature (19°C–22°C) and humidity (40%–50%) on a 12-hour light/12-hour dark cycle.

Abs, immunofluorescence, and immunohistochemistry. The Abs used were the anti-Htt Abs mAb 2B4 (1:500; Euromedex), mAb 4C8 (1:500; Euromedex), and polyclonal Ab (pAb) SE3619 (1:100; ref. 18); the mAbs anti–α-tubulin DM1A (1:1,000; Sigma-Aldrich), anti–N-acetyl tubulin (6-11B1, 1:200; Sigma-Aldrich), anti–γ-tubulin GTU88 (1:100; Sigma-Aldrich), and anti-GFAP (G3893, 1:1,000; Sigma-Aldrich); and the pAb anti–adenylyl cyclase III (1:4,000, catalog no. sc-588; Santa Cruz). Anti-PCM1 (1:4,000; ref. 9) and anti-ninein (1:3,000; ref. 19) Abs were gifts from A. Merdes (CNRS, Toulouse, France) and M. Bornens (Institut Curie, Paris, France), respectively. The pAb HAP1 (784) Ab was generated by injection of the peptide CATHSPSAREEEGPSGAT (rat HAP1B amino acid sequence 613–629) into rabbits. pAbs were characterized as previously described (18). This Ab worked only in immunofluorescence (1:1,000) and was validated using siRNA-HAP1 in cells (see Figure 3).

For immunofluorescence, cells were grown on glass coverslips coated either with fibronectin (striatal cell and primary neurons) or with poly-D-lysine plus laminin (astrocytes), transfected, and fixed either with cold methanol (–20°C) or with 4% PFA in PBS. Membrane-associated proteins were pre-extracted in PHEM buffer before fixation in cold methanol. Secondary Abs used were goat anti-mouse and anti-rabbit conjugated to Alexa Fluor 488, Alexa Fluor 555, or Alexa Fluor 647 (Invitrogen) at 1:200. Immunofluorescence images were acquired on a Leica DMRXA equipped for 3D acquisitions with a 100× NA 1.4 objective.

For immunohistochemistry on *Hdh*$^{+/+}$ and *Hdh*$^{Q111/Q111}$ mice, mice were transcardially perfused with 4% paraformaldehyde in 0.1 M sodium phosphate (pH 7.4). Coronal sections (14 μm) were incubated overnight at 4°C with anti-PCM1 (1:2,000) and anti–N-acetylated tubulin (1:200) Abs. Posterior coronal sections (5 μm) of P15 old *Wnt-Cre/+;Hdh*$^{fl/-}$ mouse brains embedded in paraffin were deparaffinated and treated with 50 mM Tris plus 2 mM EDTA (pH 9.0) for 30 minutes at 90°C for antigen enhancement. Sections were then processed as described previously (18). For neuroblast immunohistochemistry, coronal sections were incubated with anti-goat DCX (1:200, catalog no. sc-8066; Santa Cruz), washed, and incubated in biotinylated horse anti-goat IgG (H+L) Ab (1:200, BA-9500; Vector Labs). The signal was next amplified using VECTASTAIN ABC Kit (Vector Labs). Sections were counterstained with cresyl violet.

Immunoprecipitations and immunoblotting. GFP-HAP1–stable transfected PC12 and ST*Hdh* cells were lyzed and/or used for immunoprecipitation experiments as previously described (4). The following Abs and dilutions were used: mAbs anti-Htt 4C8 (1:5,000), HA (1:500, 12CA5; BabCo), anti-p150^{Glued} (1:1,000), anti–α-tubulin (DM1A, 1:1,000), and anti-GFP (1:2,000; Roche), and pAb anti-PCM1 (1:2,000) with secondary HRP-conjugated goat anti-mouse or anti-rabbit Abs (Amersham) at 1:10,000.

Human brain tissue specimen processing, immunostaining, and immunoblotting. Postmortem striatal tissue specimens from 24 adult-onset HD patients (7 grade 2, 9 grade 3, and 8 grade 4; mean age of death, 67.2 years; range, 59–70 years) and 8 age-matched patients without any known neurological symptoms (mean age, 68.9 years; range 60–78 years) were dissected fresh and flash frozen. Brain tissue specimens were collected at the Bedford Veterans Administration Medical Center Brain Tissue Archive. The postmortem intervals were similar for controls and HD patients (mean time, 12.2 hours; range, 4–18 hours). The mean number of CAG repeats on the HD specimens was 43.1 (range, 41–45 CAG repeats). Each HD patient had been clinically diagnosed based on known family history and phenotypic symptoms of HD, confirmed by neuropathological examination and graded by severity (25). Fixed striatal tissue blocks were placed in cold cryoprotectant in increasing concentrations of 10% and 20% glycerol, 2% DMSO solution, for 24–36 hours. Striatal sections of human HD and normal control tissue specimens with the ependymal lateral ventricle zone intact were incubated with anti-PCM1 and anti–N-acetylated tubulin Abs as described above, washed in PBS, incubated with horse anti-rabbit FITC conjugate (1:500; Vector) and donkey anti-mouse Cy3 conjugate (1:500; Jackson Immunoresearch Laboratories), and examined using a Nikon Eclipse E800 fluorescent microscope.

Western blot analyses in neostriatal tissue specimens were performed on all 24 HD patients and 8 age-matched control subjects. Brain lysates from the medial caudate nucleus at the ependymal border were obtained by fractionating tissue samples in 100 mM Tris (pH 7.4) lysis buffer. Protein extracts were immunoblotted for PCM1 and α-tubulin. Results were standardized to α-tubulin and analyzed using NIH Image J (http://rsb.info.nih.gov/ij/).

FRAP experiments and cell video recording. ST*Hdh*$^{+/+}$ cells were transfected with GFP-Htt480-17Q construct and mCherry-centrin1. 48 hours later, MTs were depolymerized by 5 μM nocodazole (1 hour). FRAP and video recording were performed on a LEICA DM IRBE microscope equipped with a Plan APO oil ×100 (NA 1.4) objective and recorded with a Photometrics CoolSNAP HQ2 camera (Roper Scientific). A Laser diode 488 nm/200 mW was used for photobleaching (Coherent Sapphire Laser). Images were collected in stream set at 2 × 2 binning with an exposure time of 50–150 ms with a *Z* step of 0.3 μm. The GFP-Htt480-17Q–labeled centrosome was bleached during 5 ms, and fluorescence recovery at the centrosome was followed for up to 300 minutes after bleach, acquiring stack images every 5–10 minutes. For PCM1 dynamics, ST*Hdh*$^{+/+}$ and ST*Hdh*$^{Q109/Q109}$ cells were transfected with PCM1-GFP and analyzed as described above.

Scanning electron microscopy and ciliary tuft orientation and length. Dissection and preparation of the samples were done as previously described (24). Samples were next mounted, sputter-coated with gold-palladium, and examined with a JEOL JSM 6700F scanning electron microscope. Cilia lengths were measured using Image J software (5–10 cilia per field, 4–10 fields per animal). Left and/or right ventricles of 2–4 animals (aged about 18–20 months) per genotype were analyzed. Measurements were performed in the posterior-dorsal region of the ventricle. Ciliary tuft orientations were calculated by measuring the orientation angle of the tuft relative to the theoretical direction of the flow using ImageJ software.

Video recording of ependymal flow. Brains from 1-year-old mice were placed into a solution of PBS 0.6% sucrose with 1:1,000 dilution of FluoSpheres carboxylate-modified microspheres 1 μm in diameter (F8823; Invitrogen). Thick coronal sections (0.5 mm) containing the lateral ventricles were made at the level of 4 mm interaural point. We used sections in which

we observed, from an anterior view, the presence of the anterior commissures, and from a posterior view the septofimbrial nucleus and fimbria. Video tracking was performed using an AxioCam MRm camera attached to a Zeiss Lumar V12 stereomicroscope. Recording was done with a 20-ms exposure time at ×150 magnification for 2 minutes using AxioVision 4.7 software. Videos of fluorescent particles were binarized to calculate the number and trajectories of particles using the ImageJ plug-in "ParticleTracker" (37), and kymographs were generated using a homemade ImageJ KymoToolbox plug-in.

Statistics. All data are expressed as mean ± SEM. 1-tailed Student's *t* test was used for single comparisons. Multiple comparisons were performed by 1-way ANOVA with Fisher's post-hoc analyses (Statview 4.5 software; SAS Institute Inc.). See Supplemental Methods for details. A *P* value less than 0.05 was considered significant.

Study approval. All animal experimental procedures were performed in strict accordance with the recommendations of the European Community (86/609/EEC) and the French National Committee (87/848) for care and use of laboratory animals. Written informed consent for use of the human tissue specimens was given, and the study was approved by the review board at the Bedford VA Medical Center.

Acknowledgments

We acknowledge S. Humbert for support and discussions; C. Janke, R. Roy, A. Sawa, and S. Zeitlin for discussions; S. Guadagnini and Institut Pasteur PFMU for help in scanning electron microscopy; and members of the Saudou and Humbert laboratories for helpful comments. This work was supported by grants from Agence Nationale pour la Recherche (ANR-08-MNP-039, to F. Saudou), Association pour la Recherche sur le Cancer (ARC 4950, to F. Saudou), and Fondation pour la Recherche Médicale (FRM, to F. Saudou), NIH (grants NS058793 and NS066912, to R.J. Ferrante), the Veterans Administration (VISN 1, to R.J. Ferrante), CNRS, INSERM, and Institut Curie (to F. Saudou). J.R. Pineda was supported by fundación F.E.C.Y.T. and Institut Curie. G. Liot was supported by CHDI Foundation Inc. and Fondation Pierre-Gilles de Gennes pour la Recherche. G. Keryer is a CNRS investigator. F. Saudou is an INSERM investigator.

Received for publication February 14, 2011, and accepted in revised form August 24, 2011.

Address correspondence to: Frédéric Saudou, Institut Curie, CNRS UMR 3306, INSERM U1005, F-91405 Orsay, France. Phone: 33.1.69.86.30.24; Fax: 33.1.69.86.30.17; E-mail: Frederic.Saudou@curie.fr.

Jose R. Pineda's present address is: Laboratoire de Radiopathologie, CEA-DSV/DRR, IPSC, Fontenay-aux-Roses, France.

1. Borrell-Pages M, Zala D, Humbert S, Saudou F. Huntington's disease: from huntingtin function and dysfunction to therapeutic strategies. *Cell Mol Life Sci*. 2006;63(22):2642–2660.
2. Caviston JP, Ross JL, Antony SM, Tokito M, Holzbaur EL. Huntingtin facilitates dynein/dynactin-mediated vesicle transport. *Proc Natl Acad Sci U S A*. 2007;104(24):10045–10050.
3. Gauthier LR, et al. Huntingtin controls neurotrophic support and survival of neurons by enhancing BDNF vesicular transport along microtubules. *Cell*. 2004;118(1):127–138.
4. Colin E, et al. Huntingtin phosphorylation acts as a molecular switch for anterograde/retrograde transport in neurons. *EMBO J*. 2008;27(15):2124–2134.
5. Engelender S, et al. Huntingtin-associated protein 1 (HAP1) interacts with the p150Glued subunit of dynactin. *Hum Mol Genet*. 1997;6(13):2205–2212.
6. Li SH, Gutekunst CA, Hersch SM, Li XJ. Interaction of huntingtin-associated protein with dynactin P150Glued. *J Neurosci*. 1998;18(4):1261–1269.
7. Pardo R, Molina-Calavita M, Poizat G, Keryer G, Humbert S, Saudou F. pARIS-htt: an optimised expression platform to study huntingtin reveals functional domains required for vesicular trafficking. *Mol Brain*. 2010;3:17.
8. Goetz SC, Anderson KV. The primary cilium: a signalling centre during vertebrate development. *Nat Rev Genet*. 2010;11(5):331–344.
9. Dammermann A, Merdes A. Assembly of centrosomal proteins and microtubule organization depends on PCM-1. *J Cell Biol*. 2002;159(2):255–266.
10. Kim J, Krishnaswami SR, Gleeson JG. CEP290 interacts with the centriolar satellite component PCM-1 and is required for Rab8 localization to the primary cilium. *Hum Mol Genet*. 2008;17(23):3796–3805.
11. Nachury MV, et al. A core complex of BBS proteins cooperates with the GTPase Rab8 to promote ciliary membrane biogenesis. *Cell*. 2007;129(6):1201–1213.
12. Kulaga HM, et al. Loss of BBS proteins causes anosmia in humans and defects in olfactory cilia structure and function in the mouse. *Nat Genet*. 2004;36(9):994–998.
13. Johanson CE, Duncan JA 3rd, Klinge PM, Brinker T, Stopa EG, Silverberg GD. Multiplicity of cerebrospinal fluid functions: New challenges in health and disease. *Cerebrospinal Fluid Res*. 2008;5:10.
14. Banizs B, et al. Dysfunctional cilia lead to altered ependyma and choroid plexus function, and result in the formation of hydrocephalus. *Development*. 2005;132(23):5329–5339.
15. Ibanez-Tallon I, Gorokhova S, Heintz N. Loss of function of axonemal dynein Mdnah5 causes primary ciliary dyskinesia and hydrocephalus. *Hum Mol Genet*. 2002;11(6):715–721.
16. Dietrich P, Shanmugasundaram R, Shuyu E, Dragatsis I. Congenital hydrocephalus associated with abnormal subcommissural organ in mice lacking huntingtin in Wnt1 cell lineages. *Hum Mol Genet*. 2009;18(1):142–150.
17. Trettel F, et al. Dominant phenotypes produced by the HD mutation in STHdh(Q111) striatal cells. *Hum Mol Genet*. 2000;9(19):2799–2809.
18. Godin JD, et al. Huntingtin is required for mitotic spindle orientation and mammalian neurogenesis. *Neuron*. 2010;67(3):392–406.
19. Azimzadeh J, Bornens M. Structure and duplication of the centrosome. *J Cell Sci*. 2007;120(pt 13):2139–2142.
20. Martin EJ, et al. Analysis of Huntingtin-associated protein 1 in mouse brain and immortalized striatal neurons. *J Comp Neurol*. 1999;403(4):421–430.
21. Li XJ, et al. A huntingtin-associated protein enriched in brain with implications for pathology. *Nature*. 1995;378(6555):398–402.
22. Domire JS, Mykytyn K. Markers for neuronal cilia. *Methods Cell Biol*. 2009;91:111–121.
23. Wheeler VC, et al. Early phenotypes that presage late-onset neurodegenerative disease allow testing of modifiers in Hdh CAG knock-in mice. *Hum Mol Genet*. 2002;11(6):633–640.
24. Mirzadeh Z, Merkle FT, Soriano-Navarro M, Garcia-Verdugo JM, Alvarez-Buylla A. Neural stem cells confer unique pinwheel architecture to the ventricular surface in neurogenic regions of the adult brain. *Cell Stem Cell*. 2008;3(3):265–278.
25. Vonsattel JP, Myers RH, Stevens TJ, Ferrante RJ, Bird ED, Richardson EP Jr. Neuropathological classification of Huntington's disease. *J Neuropathol Exp Neurol*. 1985;44(6):559–577.
26. Sawamoto K, et al. New neurons follow the flow of cerebrospinal fluid in the adult brain. *Science*. 2006;311(5761):629–632.
27. Kim JC, et al. The Bardet-Biedl protein BBS4 targets cargo to the pericentriolar region and is required for microtubule anchoring and cell cycle progression. *Nat Genet*. 2004;36(5):462–470.
28. Dragatsis I, Zeitlin S, Dietrich P. Huntingtin-associated protein 1 (Hap1) mutant mice bypassing the early postnatal lethality are neuroanatomically normal and fertile but display growth retardation. *Hum Mol Genet*. 2004;13(24):3115–3125.
29. Badano JL, Teslovich TM, Katsanis N. The centrosome in human genetic disease. *Nat Rev Genet*. 2005;6(3):194–205.
30. Sheng G, et al. Huntingtin-associated protein 1 interacts with Ahi1 to regulate cerebellar and brainstem development in mice. *J Clin Invest*. 2008;118(8):2785–2795.
31. Liu Q, et al. The proteome of the mouse photoreceptor sensory cilium complex. *Mol Cell Proteomics*. 2007;6(8):1299–1317.
32. Lazic SE, et al. Olfactory abnormalities in Huntington's disease: decreased plasticity in the primary olfactory cortex of R6/1 transgenic mice and reduced olfactory discrimination in patients. *Brain Res*. 2007;1151:219–226.
33. Fang Q, et al. Brain-specific proteins decline in the cerebrospinal fluid of humans with Huntington disease. *Mol Cell Proteomics*. 2009;8(3):451–466.
34. Lancaster MA, Schroth J, Gleeson JG. Subcellular spatial regulation of canonical Wnt signalling at the primary cilium. *Nat Cell Biol*. 2011;13(6):700–707.
35. Godin JD, Poizat G, Hickey MA, Maschat F, Humbert S. Mutant huntingtin-impaired degradation of beta-catenin causes neurotoxicity in Huntington's disease. *EMBO J*. 2010;29(14):2433–2445.
36. Li SH, et al. Lack of huntingtin-associated protein-1 causes neuronal death resembling hypothalamic degeneration in Huntington's disease. *J Neurosci*. 2003;23(17):6956–6964.
37. Sbalzarini IF, Koumoutsakos P. Feature point tracking and trajectory analysis for video imaging in cell biology. *J Struct Biol*. 2005;151(2):182–195.